

Nonlinear traveling waves as a framework for understanding turbulent drag reduction

By **Wei Li, Li Xi and Michael D. Graham**

Department of Chemical and Biological Engineering
University of Wisconsin-Madison, Madison, WI 53706-1691

(Received 22 September 2018)

Nonlinear traveling waves that are precursors to laminar-turbulent transition and capture the main structures of the turbulent buffer layer have recently been found to exist in all the canonical parallel flow geometries. We study the effect of polymer additives on these “exact coherent states” (ECS), in the plane Poiseuille geometry. Many key aspects of the turbulent drag reduction phenomenon are found, including: delay in transition to turbulence; drag reduction onset threshold; diameter and concentration effects. Furthermore, examination of the ECS existence region leads to a distinct prediction, consistent with experiments, regarding the nature of the maximum drag reduction regime. Specifically, at sufficiently high wall shear rates, viscoelasticity is found to completely suppress the normal (*i.e.* streamwise-vortex-dominated) dynamics of the near wall region, indicating that the maximum drag reduction regime is dominated by a distinct class of flow structures.

1. Introduction

The reduction of turbulent drag by polymer additives has received much attention since it was first observed experimentally in 1940s (See reviews by Lumley (1969); Virk (1975);

McComb (1990); Graham (2004)). For a given flow rate, small polymer concentrations, on the order of ten parts per million by weight, can reduce the pressure drop in pipe or channel flow, for example, by 50% or greater. After six decades of research, the subject remains an active area of research, in part because of applications but also because it lies at the intersection of two complex and important fields, turbulence and polymer dynamics. A better understanding of this phenomenon may in turn yield insights into both the dynamics of drag-reducing fluids and of turbulent flows. The goal of the present work is to address turbulent drag reduction in the context of the dominant structures in the turbulent buffer layer, an approach which turns out to touch on many key aspects of the drag reduction phenomenon.

We focus here on pressure-driven channel flow with average wall shear stress τ_w , of a fluid with dynamic viscosity η_s (in the absence of polymer), density ρ and kinematic viscosity $\nu = \eta_s/\rho$. The average streamwise velocity U_{avg} and half-channel height l define outer scales for the flow. Inner scales are the friction velocity $u_\tau = \sqrt{\tau_w/\rho}$ and the near-wall length scale $l_w = \nu/u_\tau$. As usual, quantities expressed in terms of these so-called “wall units” are denoted with a superscript $+$. The friction Reynolds number $Re_\tau = u_\tau l/\nu$ is simply the half channel height expressed in wall units. The Weissenberg number is denoted $Wi = \lambda \dot{\gamma}_w = \lambda u_\tau^2/\nu$, where λ is polymer relaxation time and $\dot{\gamma}_w$ is the average wall shear rate. Experimental results for a given fluid and flow geometry lie on curves of constant elasticity parameter $El = 2\lambda\nu/l^2$.

In channel or pipe flow, drag reduction results are often represented on a Prandtl-von Karman plot, U_{avg}/u_τ vs. $\log Re_\tau$ ($\sim \log Wi - \log El$), shown schematically in Fig. 1a. Point A corresponds to transition to turbulence, which in Newtonian flow occurs at $Re_\tau \approx 45$ (Carlson *et al.* 1982). One typical experimental path for a given polymer solution and channel size is shown by the curve labeled “exp1”. Along this path, once Re_τ

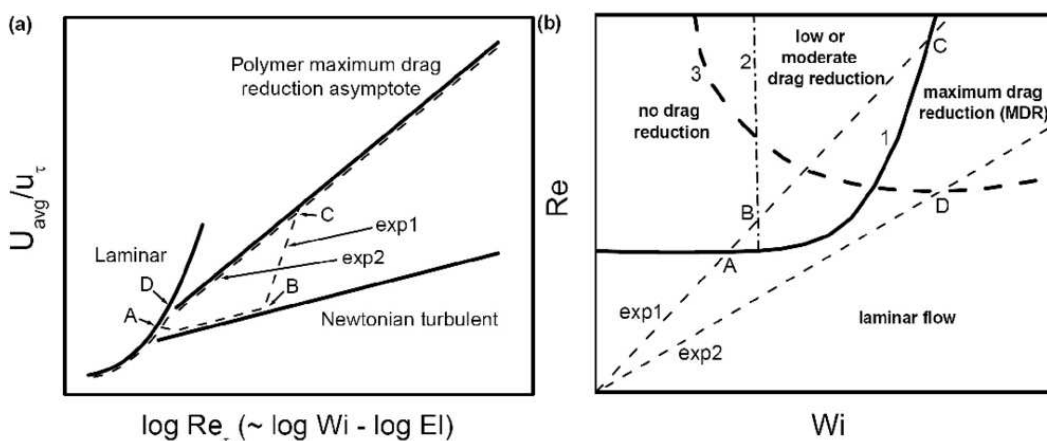


FIGURE 1. (a) Schematic Prandtl-von Karman plot. The dashed lines represent the experimental paths by which specific polymer systems of different molecular weights, concentrations, polymer-solvent pairs, etc., approach the maximum drag reduction asymptote. (b) Schematic of polymer induced turbulent drag reduction based on existence regions for nonlinear coherent states.

exceeds a critical value (point B), the slope of the data increases from the Newtonian value, indicating onset of drag reduction. As Re_{τ} increases, data eventually approaches a new curve at point C . This curve, the so-called Maximum Drag Reduction (MDR) asymptote, is insensitive to polymer concentration, molecular weight or polymer species – all results collapse onto it at large Re_{τ} ; it is a universal feature of drag reduction by polymers. For large channels or low polymer concentrations, the value of Re_{τ} at the onset of drag reduction is independent of polymer concentration and corresponds to a critical Weissenberg number. For small channels or large concentrations, however, diameter and concentration effects have been observed experimentally (Virk 1975): specifically, there exists a critical pipe diameter below which, or a critical polymer concentration above which the flow behavior directly transits from laminar flow to the maximum drag reduction curve as Re_{τ} increases. An experimental path showing this effect is labeled “exp2”; transition from laminar flow to MDR occurs at point D .

Studies of drag-reducing fluids indicate that near the onset of drag reduction, the effects of the polymer are confined primarily to the buffer layer region of the flow (Virk 1975; Donohue *et al.* 1972). Experimental observations and DNS studies show that the dominant structures in the buffer layer are pairs of counter-rotating, streamwise-aligned vortices (Robinson 1991; Jeong *et al.* 1997). These vortices pull slower moving fluids away from the wall, forming low-speed, streamwise velocity streaks. In drag-reducing flows, these structures are modified by polymers: the buffer region thickens (Virk 1975), the coherent structures in this region shift to larger scales (Donohue *et al.* 1972; Sureshkumar *et al.* 1997; den Toonder *et al.* 1997), and the bursting rate decreases (Donohue *et al.* 1972). Recent experimental results (Warholic *et al.* 1999, 2001) reveal that in the maximum drag reduction region the ejections from the wall are eliminated and the near-wall vortices that sustain turbulence in a Newtonian fluid are completely destroyed. Low-speed streamwise velocity streaks are essentially absent. These observations suggest that the coherent structures in buffer layer region are crucial in addressing rheological drag reduction in wall-bounded turbulent flows.

A recent advance in the understanding of these important near-wall structures has come with the recognition that, in all the canonical parallel geometries (plane Couette, plane Poiseuille, pipe) the Navier-Stokes equations support nonlinear traveling wave states, the family of so-called “exact coherent states” or ECS (Nagata 1986; Clever & Busse 1997; Waleffe 1998, 2001, 2003; Faisst & Eckhardt 2003; Wedin & Kerswell 2004). Jiménez and coworkers (Jiménez & Pinelli 1999; Jiménez & Simens 2001) have found related states in spatially filtered direct numerical simulations (DNS), showing the autonomous nature of the near-wall behavior. The flow structure of these states is a mean shear and a pair of staggered streamwise-aligned counter-rotating vortices, as is found in the turbulent buffer layer. In the plane Poiseuille geometry, ECS come into existence at Re_τ of 44.2

(Waleffe 2003), very close to the experimentally observed Re_τ of ~ 45 for the transition to turbulence (Carlson *et al.* 1982). The spanwise wavelength $L_z^+ = 105.5$ of the ECS at onset closely matches the streak spacing of ~ 100 wall-units widely observed in experiments over a large range of Reynolds numbers (Robinson 1991). Direct numerical simulations of turbulence in “minimal channel flow”, *i.e.*, flow in the smallest computational domain that reproduces the velocity field statistics of near-wall turbulence, give a range for the streamwise length L_x^+ of 250–350, compared to $L_x^+ = 273.7$ for the ECS, and a spanwise length that is again approximately 100 wall units (Jiménez & Moin 1991). It should be pointed out that this minimum channel contains a single wavelength of a wavy streak and a pair of quasi-streamwise vortices, which is the same structure seen in the ECS. A conditional sampling study of coherent structures in a larger scale DNS (Jeong *et al.* 1997) indicates that the dominant structures near the wall in turbulent channel flow are counter-rotating, streamwise-aligned vortices with a streamwise length $L_x^+ \sim 250$, a spanwise length $L_z^+ \sim 100$ and a wall-normal size of $y^+ \sim 50$, which agrees with the scales of the ECS at onset. The ECS also capture the location of the peak, at $y^+ \approx 12$, in the production of turbulent kinetic energy for wall-bounded turbulence (Kim *et al.* 1987; Li *et al.* 2005). In short, the ECS are precursors to turbulence and their structure and length scales closely match experimentally observed near-wall behavior.

Because the first effects of polymer arise in the buffer region, whose structure the ECS evidently capture, these flows provide a natural starting point for understanding drag reduction. In prior work, we have studied the initial effects of viscoelasticity on ECS in the plane Couette and plane Poiseuille geometries (Stone *et al.* 2002; Stone & Graham 2003; Stone *et al.* 2004; Li *et al.* 2005). The primary effect was found to be the weakening of the streamwise vortices, as well as changes in the statistics of the velocity fluctuations that are consistent with experimental observations at low levels of drag reduction. The

present work takes a broader view, examining the region of parameter space (Re , Wi) in which ECS exist and its connection to experimental observations.

2. Formulation

We consider pressure-driven flow with no-slip boundary conditions; v_x , v_y , and v_z are streamwise, wall-normal, and spanwise components of the velocity, \mathbf{v} , respectively. Reflection symmetry is imposed at the channel centerline. The laminar centerline velocity, U , and the half-channel height, l , are used to scale velocity and position, respectively. The average wall shear rate $\dot{\gamma}_w$ is given by $2U/l$. Time, t , is scaled with l/U , and pressure, p , with ρU^2 . The stress due to the polymer, $\boldsymbol{\tau}_p$, is nondimensionalized with the polymer elastic modulus, $G = \eta_p/\lambda$, where η_p is the polymer contribution to the zero-shear rate viscosity. The momentum balance and the equation of continuity are

$$\frac{D\mathbf{v}}{Dt} = -\nabla p + \beta \frac{1}{Re} \nabla^2 \mathbf{v} + (1 - \beta) \frac{2}{Re Wi} (\nabla \cdot \boldsymbol{\tau}_p), \quad (2.1)$$

$$\nabla \cdot \mathbf{v} = 0. \quad (2.2)$$

Here $\beta = \eta_s/(\eta_s + \eta_p)$ is the fraction of the total zero-shear viscosity that is due to the solvent, $Re = \frac{\rho U l}{\eta_s + \eta_p}$ and $Re_\tau = \sqrt{2Re}$.

The polymer stress is computed with the widely-used FENE-P constitutive model (Bird *et al.* 1987):

$$\frac{\boldsymbol{\alpha}}{1 - \frac{tr\boldsymbol{\alpha}}{b}} + \frac{Wi}{2} \left(\frac{D\boldsymbol{\alpha}}{Dt} - \boldsymbol{\alpha} \cdot \nabla \mathbf{v} - \nabla \mathbf{v}^T \cdot \boldsymbol{\alpha} \right) = \frac{b\boldsymbol{\delta}}{b+2}, \quad (2.3)$$

where $\boldsymbol{\alpha}$ is a non-dimensional conformation tensor and b is proportional to the maximum extension of the dumbbell — $tr\boldsymbol{\alpha}$ cannot exceed b . The polymer contribution to the stress is given by:

$$\boldsymbol{\tau}_p = \frac{b+5}{b} \left(\frac{\boldsymbol{\alpha}}{1 - \frac{tr\boldsymbol{\alpha}}{b}} - \left(1 - \frac{2}{b+2} \right) \boldsymbol{\delta} \right). \quad (2.4)$$

The extensibility parameter $Ex = \frac{2b(1-\beta)}{3\beta}$ measures the relative magnitude of the poly-

mer and solvent contributions to the steady state extensional stress in uniaxial extension at high extension rate. We consider the situation $1 - \beta \ll 1$, in which case shear-thinning is negligible, as the polymer only contributes a very small amount to the total shear viscosity of the solution. In this situation, significant effects of the polymer on the flow are expected only when $Ex \gg 1$. Finally, recall that experimental results for a given fluid and flow geometry lie on curves of constant elasticity parameter $El = 2\lambda\nu/l^2 = Wi/Re$.

The conservation and constitutive equations are solved through a Picard iteration in a traveling reference frame – the wave speed is part of the solution. A Newtonian ECS, as computed in Waleffe (1998), is first used to calculate the polymer stress tensor, $\boldsymbol{\tau}_p$, by inserting the velocity field in the evolution equation for $\boldsymbol{\alpha}$ and integrating for a short length of time, usually one time unit (l/U). For this $\boldsymbol{\tau}_p$, a steady state of the momentum and continuity equations is found by Newton iteration. The resulting velocity field, \mathbf{v} , is used to compute the new $\boldsymbol{\tau}_p$, and the process is repeated until the velocity and polymer field converge to a steady state.

The momentum and continuity equations are discretized using a Fourier-Chebyshev formulation with typically a $9 \times 17 \times 9$ grid. The conformation tensor, $\boldsymbol{\alpha}$, is discretized with a third-order, compact upwind difference scheme (Lele 1992; Min *et al.* 2001) in the x and z directions and Chebyshev collocation in the y direction. In this as in most previous computational studies of polymers in turbulent flows, we have found it necessary to add an artificial stress diffusion term $\frac{1}{ScRe} \nabla^2 \boldsymbol{\alpha}$, to the right-hand side of Eq. (2.3) to achieve numerical stability. The Schmidt number, Sc , which is the ratio of the momentum diffusivity to stress diffusivity, is set to value of 1.0. This value of Sc , though artificially small, is greater or of the same order of magnitude as that used in many DNS studies (Sureshkumar *et al.* 1997; Ptasinski *et al.* 2003; Sureshkumar & Beris 1995; Sibilla & Baron 2002). In the range of Sc where solutions can be obtained, the bifurcation

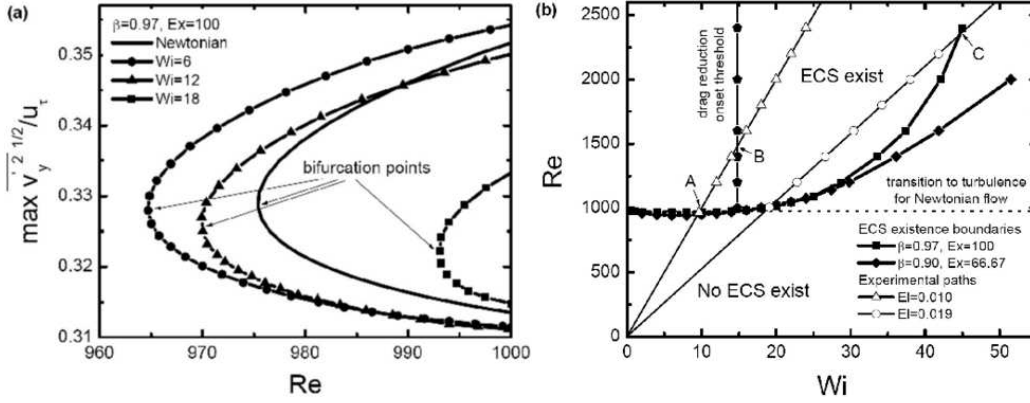


FIGURE 2. (a) Bifurcation diagram for Newtonian and viscoelastic ECS. (b) Existence boundaries and drag reduction regimes for viscoelastic ECS. For all results, $L_x = 2\pi/1.0148$ and $L_z = 2\pi/2.633$.

diagrams shown below are insensitive to its value. The stress diffusion term is integrated implicitly by the Crank-Nicholson method with the other terms of the equation integrated using the Adams-Bashforth method. This equation is solved on a finer mesh than the momentum, continuity pair, typically $48 \times 49 \times 48$.

3. Results and discussion

We study the Newtonian and viscoelastic ECS at fixed streamwise and spanwise lengths: $L_x = 2\pi/1.0148$ and $L_z = 2\pi/2.633$ (*i.e.*, $L_x^+ = 273.7$ and $L_z^+ = 105.5$ at $Re_\tau = 44.2$). This wavelength pair is where ECS first come into existence in the Newtonian case. The trivial base state in this geometry (laminar Poiseuille flow) exists at all Re . At $Re \approx 977$ ($Re_\tau = 44.2$) for the Newtonian flow, two new solutions appear via a saddle-node bifurcation as shown in Fig. 2a. These are the ECS. These solutions are plotted using the maximum in the root mean square wall-normal velocity fluctuations for the solution, $\overline{v_y'^2}^{1/2}$. (Hereafter, an overbar indicates that the variable is averaged over the streamwise and spanwise directions.) The solutions with higher maximum wall-normal

velocity at a given Re are called “high drag” solutions due to their lower mean velocity at the centerline of the channel compared to the “low drag” solutions. All results in this paper are for the “high drag” states. Although both solutions are unstable, their status as precursors to transition and their structural similarity to buffer layer turbulence suggest that they are saddle points that underlie in part the strange attractor of turbulent flow.

Fig. 2a indicates that the addition of polymer changes the Reynolds number Re_{\min} at which the ECS come into existence. Curves of ECS existence boundaries Re_{\min} vs. Wi are given for two parameter sets by the thick solid curves on Fig. 2b. These separate the region where the ECS can exist (above the curves) from the region where no ECS exist, for the given value of Ex . While at low Wi , there is a slight decrease in Re_{\min} from the Newtonian value, once Wi exceeds 45, Re_{\min} for $Ex = 100$ is more than doubled. This dramatic increase in Re_{\min} after onset is consistent with the experimental observation that the transition to turbulence in a polymer solution is delayed to higher Re than in the Newtonian case (Giles & Pettit 1967; White & McEligot 1970; Escudier *et al.* 1999). We will refer to the Wi above which Re_{\min} for the viscoelastic ECS is greater than for the Newtonian ECS as the onset Weissenberg number Wi_{onset} for drag reduction. Fig. 2b shows that $Wi_{\text{onset}} \approx 15$, a value which is insensitive to polymer extensibility (Ex) or concentration (β). Furthermore, in simulations at constant Re , it is found that the value where the centerline mean velocity U_{\max} first exceeds the Newtonian value – the nearly vertical set of points in Fig. 2b – is also located at $Wi \approx 15$ in the parameter regime that has been examined here. This onset value is high by about a factor of two compared to values predicted by two recent viscoelastic DNS studies (Housiadas & Beris 2003; Min *et al.* 2003), but in those studies El was significantly smaller, and the onset Reynolds number correspondingly larger, than the values considered here.

Figure 3a shows mean velocity profiles at six different sets of parameter values, each

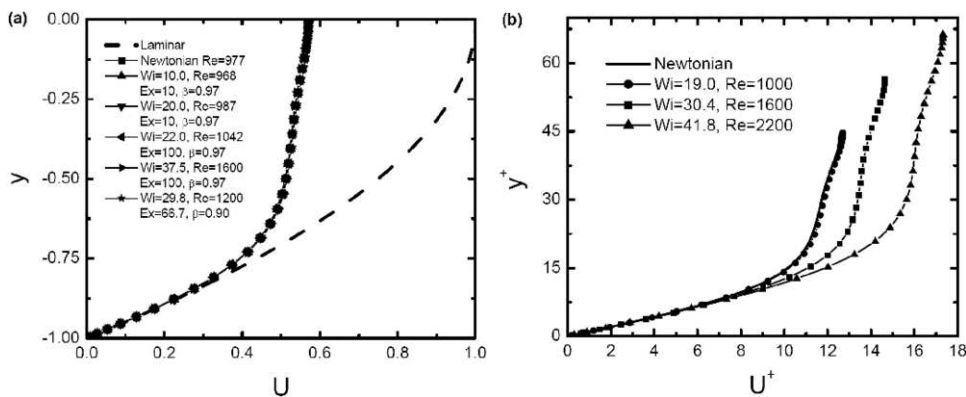


FIGURE 3. Mean streamwise velocity for Newtonian and viscoelastic ECS on the ECS existence boundary.

corresponding to a point on the existence boundary for the ECS (*i.e.* a bifurcation point). Remarkably, they all fall on the same curve, when plotted in outer units. Therefore, at least for the values of Re and Wi that are currently accessible in our simulations, we observe that mean velocity profiles at onset of the ECS have a universal form.

We now turn to the study of the evolution of the ECS along some experimental paths, lines of constant El . Two such paths, the thin solid lines with hollow symbols, are shown in Fig. 2b. Consider first the case $El = 0.010$; as Re and Wi increase, the path intersects the ECS existence boundary at point A and the drag reduction onset threshold curve at point B , where the transition to turbulence and the onset of drag reduction occur, respectively. Turning to the case $El = 0.019$, mean velocity profiles expressed in wall units are shown for various values of Re in Fig. 3b. For this parameter set, drag reduction is observed immediately upon onset of the ECS. Along with drag reduction, enhanced streamwise velocity fluctuations and the reduced wall-normal and spanwise velocity fluctuations are found, consistent with experimental observations and DNS results at low to moderate degrees of drag reduction (Virk 1975; Sureshkumar *et al.* 1997). The effect of viscoelasticity can also be observed in the reduced Reynolds shear stress and

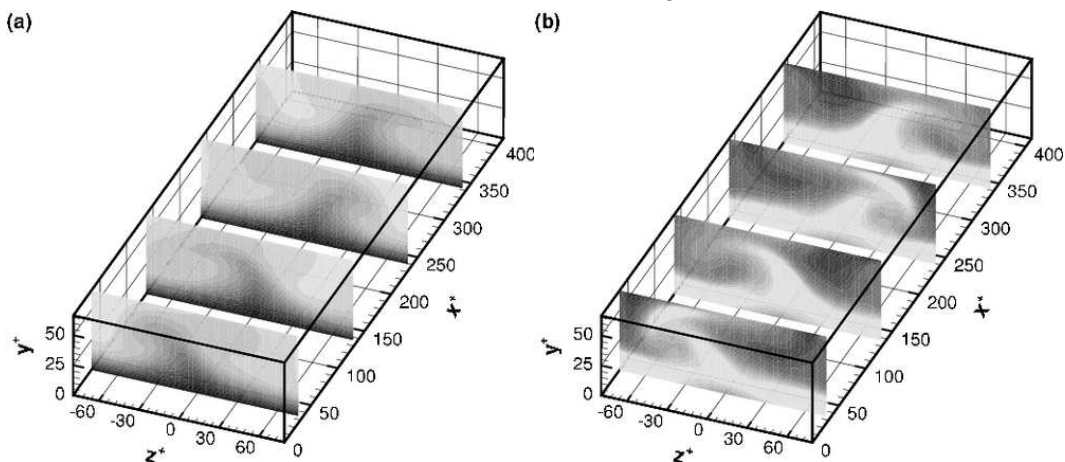


FIGURE 4. (a) Streamwise velocity for an exact coherent state at $Re = 2200 (Re_\tau = 66.3)$, $Wi = 41.8$, $Ex = 100$, $\beta = 0.97$. Range: 0 (black) – 0.58 (white). (b) Trace of the polymer stress for the same state. Range: 0 (black) – 1800 (white).

ultimately can be traced to the suppression of the streamwise vortices by the viscoelasticity (Stone *et al.* 2002, 2004; Li *et al.* 2005). Figure 4 shows fields of v_x and $\text{tr}\tau_p$ on the $El = 0.019$ path at $Wi = 41.8$, $Re = 2200$ (the point just left of the label “C” on Figure 2b). The region of high polymer stress clearly “wraps around” the streamwise vortices, and the corresponding polymer force ($\sim \nabla \cdot \tau_p$) is in direct opposition to the vortex motions.

Continuing upward in Re and Wi at $El = 0.019$, the path re-intersects the ECS existence boundary, at point C in Fig. 2b. (We suspect that this will also happen in the $El = 0.010$ case, but at higher Re and Wi than are accessible with our current computational approach.) Above this point the flow can no longer sustain these ECS; viscoelasticity completely suppresses the near-wall vortical structures. This result is consistent with experimental observations that, in the MDR regime, the eruptions of low-momentum fluid from the wall are eliminated and the near-wall streamwise vortices are completely destroyed (Warholic *et al.* 1999, 2001). Experimental results also show that in the MDR regime, the Reynolds shear stress is much smaller than the Newtonian

value (Warholic *et al.* 1999, 2001; Ptasinski *et al.* 2001), and streamwise velocity fluctuations decrease to levels close to or below the Newtonian value (Warholic *et al.* 1999). All these observations suggest that the turbulent production and dissipation take place by a different mechanism in the MDR regime than at lower degrees of drag reduction. Although our study does not reveal this mechanism directly, it does suggest that the disappearance of ECS is related to the MDR regime. This result encourages us to take a broader view, examining the region of parameter space (Re , Wi) in which ECS exist and its connection to experimental observations.

Fig. 1b is a schematic based on the results shown in Fig. 2b. Line 1 represents the ECS existence boundary at constant Ex . Line 2 represents the drag reduction onset threshold, which separates the ECS existence region into “turbulence without drag reduction” and “turbulence with low or moderate drag reduction” regions. Line “exp1” represents an experimental path at constant El , which passes through the ECS existence region. In this case, as Re (and Wi) increases, this path intersects with the ECS existence boundary at point A and drag reduction onset threshold at point B , where the transition to turbulence and the drag reduction onset occur, respectively. Note the correspondence with points A and B on the schematic Prandtl-von Karman plot, Fig. 1a, as well as on Fig. 2b. As Re and Wi continue to increase along this path, the system will eventually exit the ECS existence region at point C , where the flow can no longer sustain these ECS. Experimental results show that in the MDR regime, near-wall streamwise vortical structures are essentially absent. Our results together with this experimental observation suggest that the loss of ECS may be somehow related to the approach of the MDR regime, in which other types of coherent traveling wave states (temporally intermittent structures, hairpins, Tollmien-Schlichting waves, intrinsically elastic structures,...) may be unmasked and become dominant. This possibility is represented by line 3 in Fig. 1b, a hypothetical

existence boundary for a distinct class of flow structures that exists at high Wi . In this scenario, the crossing of path exp1 across point C represents the transition to the maximum drag reduction regime. This scenario, incorporating transition to turbulence, onset of drag reduction and approach of the MDR regime is consistent with the behavior on experimental path exp1 shown in Fig. 1a.

Now consider the experimental path “exp2” on Fig. 1b. This path corresponds to a value of El that does not intersect with ECS existence region at all. For the conditions $\beta = 0.97$, $Ex = 100$ shown on Fig. 2b, this situation arises if $El \gtrsim 0.024$. The scenario on Fig. 1b would predict in this case that, with the increase of Re and Wi , the flow behavior directly transits from laminar to MDR at point D . As El is inversely proportional to l^2 (or R^2 in pipe flow) this prediction is consistent with experiments in small diameter pipes – the “diameter effect” (Virk 1975), as exemplified by experimental path exp2 in Fig. 1a. The “concentration effect” can also be captured by this scenario, as we now describe. The quantity $S = 1 - \beta$ is proportional to polymer concentration in dilute solution. Using S , the parameters Ex and El can be written as $Ex = \frac{2}{3}bS/(1 - S)$ and $El = 2\lambda\eta_s/\rho l^2(1 - S)$. Thus while El is virtually unchanged by a change in S , Ex is proportional to it. An increase in Ex compresses the ECS existence boundary leftward and eventually a given experimental path can no longer intersect the ECS existence region, resulting again in flow behavior that directly transits from laminar to MDR.

Finally, we observe that the existence boundaries can be interpreted in terms of length scales. Recall that the half-height of the channel, expressed in wall units, is simply $Re_\tau = \sqrt{2Re}$. Thus the existence boundary corresponds to the minimum half-channel height in which an ECS can exist, as a function of Wi . Points where a line of constant El intersects the existence boundary are points where the channel height and the minimum height for the existence of an ECS coincide.

4. Conclusions

Many observations of drag reduction in dilute polymer solutions are mirrored by the effect of viscoelasticity on the channel flow ECS discovered by Waleffe (Waleffe 2001, 2003). The transition behaviors from laminar to turbulent flow, from no drag reduction to drag reduction, and from moderate drag reduction to MDR can be connected to the birth, evolution and death of these ECS, respectively. Our results and the scenario that we infer from them yield explicit predictions, testable by DNS, with regard to all these phenomena.

Acknowledgments

The authors are indebted to Fabian Waleffe for many illuminating discussions and for sharing his code for computation of the Newtonian exact coherent states. This work was supported by the National Science Foundation, grant CTS-0328325, and the Petroleum Research Fund, administered by the American Chemical Society.

REFERENCES

- BIRD, R. B., CURTISS, C. F., ARMSTRONG, R. C. & HASSAGER, O. 1987 *Dynamics of Polymeric Liquids*, 2nd edn., , vol. 2. New York: Wiley.
- CARLSON, D. R., WIDNALL, S. E. & PEETERS, M. F. 1982 A flow-visualization study of transition in plane Poiseuille flow. *J. Fluid Mech.* **121**, 487–505.
- CLEVER, R. M. & BUSSE, F. H. 1997 Tertiary and quaternary solutions for plane Couette flow. *J. Fluid Mech.* **344**, 137–153.
- DEN TOONDER, J. M. J., HULSEN, M. A., KUIKEN, G. D. C. & NIEUWSTADT, F. T. M. 1997 Drag reduction by polymer additives in a turbulent pipe flow: numerical and laboratory experiments. *J. Fluid Mech.* **337**, 193–231.
- DONOHUE, G. L., TIEDERMAN, W. G. & REISCHMAN, M. M. 1972 Flow visualization of the near-wall region in a drag-reducing channel flow. *J. Fluid Mech.* **50**, 559–575.

- ESCUDIER, M. P., PRESTI, F. & SMITH, S. 1999 Drag reduction in the turbulent pipe flow of polymers. *J. Non-Newtonian Fluid Mech.* **81**, 197–213.
- FAISST, H. & ECKHARDT, B. 2003 Traveling waves in pipe flow. *Phys. Rev. Lett.* **90**, 224502.
- GILES, W. B. & PETTIT, W. T. 1967 Stability of dilute viscoelastic flows. *Nature* **216**, 470–472.
- GRAHAM, M. D. 2004 Drag reduction in turbulent flow of polymer solutions. In *Rheology Reviews 2004* (ed. D. M. Binding & K. Walters), pp. 143–170. British Society of Rheology.
- HOUSIADAS, K. D. & BERIS, A. N. 2003 Polymer-induced drag reduction: Effects of variations in elasticity and inertia in turbulent viscoelastic channel flow. *Phys. Fluids* **15** (8), 2369–2384.
- JEONG, J., HUSSIAN, F., SCHOPPA, W. & KIM, J. 1997 Coherent structures near the wall in a turbulent channel flow. *J. Fluid Mech.* **332**, 185–214.
- JIMÉNEZ, J. & MOIN, P. 1991 The minimal flow unit in near wall turbulence. *J. Fluid Mech.* **225**, 221–240.
- JIMÉNEZ, J. & PINELLI, A. 1999 The autonomous cycle of near-wall turbulence. *J. Fluid Mech.* **389**, 335–359.
- JIMÉNEZ, J. & SIMENS, M. P. 2001 Low-dimensional dynamics of a turbulent wall flow. *J. Fluid Mech.* **435**, 81–91.
- KIM, J., MOIN, P. & MOSER, R. 1987 Turbulence statistics in fully developed channel flow at low Reynolds number. *J. Fluid Mech.* **177**, 133–166.
- LELE, S. K. 1992 Compact finite difference schemes with spectral-like resolution. *J. Comput. Phys.* **103**, 16–42.
- LI, W., STONE, P. A. & GRAHAM, M. D. 2005 Viscoelastic nonlinear traveling waves and drag reduction in plane poiseuille flow. *IUTAM Symposium on Laminar-Turbulent Transition and Finite Amplitude Solutions* pp. 285–308.
- LUMLEY, J. L. 1969 Drag reduction by additives. *Annu. Rev. Fluid Mech.* **1**, 367–384.
- MCCOMB, W. D. 1990 *The Physics of Fluid Turbulence*. New York: Oxford University Press.
- MIN, T., YOO, J. Y. & CHOI, H. 2001 Effect of spatial discretization schemes on numerical solution of viscoelastic fluid flows. *J. Non-Newtonian Fluid Mech.* **100**, 27–47.
- MIN, T., YOO, J. Y., CHOI, H. & JOSEPH, D. D. 2003 Drag reduction by polymer additives in a turbulent channel flow. *J. Fluid Mech.* **486**, 213–238.

- NAGATA, M. 1986 Bifurcation in Couette flow between almost corotating cylinders. *J. Fluid Mech.* **169**, 229–250.
- PTASINSKI, P. K., BOERSMA, B. J., NIEUWSTADT, F. T. M., HULSEN, M. A., VAN DEN BRULE, B. H. A. A. & HUNT, J. C. R. 2003 Turbulent channel flow near maximum drag reduction: simulations, experiments and mechanisms. *J. Fluid Mech.* **490**, 251–291.
- PTASINSKI, P. K., NIEUWSTADT, F. T. M., VAN DEN BRULE, B. H. A. A. & HULSEN, M. A. 2001 Experiments in turbulent pipe flow with polymer additives at maximum drag reduction. *Flow, Turbulence and Combustion* **66**, 159–182.
- ROBINSON, S. K. 1991 Coherent motions in the turbulent boundary layer. *Annu. Rev. Fluid Mech.* **23**, 601–639.
- SIBILLA, S. & BARON, A. 2002 Polymer stress statistics in the near-wall turbulent flow of a drag-reducing solution. *Phys. Fluids* **14** (3), 1123–1136.
- STONE, P. A. & GRAHAM, M. D. 2003 Polymer dynamics in a model of the turbulent buffer layer. *Phys. Fluids* **15**, 1247–1256.
- STONE, P. A., ROY, A., LARSON, R. G., WALEFFE, F. & GRAHAM, M. D. 2004 Polymer drag reduction in exact coherent structures of plane shear flow. *Phys. Fluids* **16**, 3470–3482.
- STONE, P. A., WALEFFE, F. & GRAHAM, M. D. 2002 Toward a structural understanding of turbulent drag reduction: nonlinear coherent states in viscoelastic shear flows. *Phys. Rev. Lett.* **89**, 208301.
- SURESHKUMAR, R. & BERIS, A. N. 1995 Effect of artificial stress diffusivity on the stability of numerical calculations and the flow dynamics of time-dependent viscoelastic flows. *J. Non-Newtonian Fluid Mech.* **60**, 53–80.
- SURESHKUMAR, R., BERIS, A. N. & HANDLER, R. 1997 Direct numerical simulation of the turbulent channel flow of a polymer solution. *Phys. Fluids* **9** (3), 743–755.
- VIRK, P. S. 1975 Drag reduction fundamentals. *AIChE J.* **21** (4), 225–256.
- WALEFFE, F. 1998 Three-dimensional coherent states in plane shear flows. *Phys. Rev. Lett.* **81** (19), 4140–4143.
- WALEFFE, F. 2001 Exact coherent structures in channel flow. *J. Fluid Mech.* **435**, 93–102.

- WALEFFE, F. 2003 Homotopy of exact coherent structures in plane shear flows. *Phys. Fluids* **15**, 1517–1534.
- WARHOLIC, M. D., HEIST, D. K., KATCHER, M. & HANRATTY, T. J. 2001 A study with particle image velocimetry of the influence of drag-reducing polymers on the structure of turbulence. *Expts. Fluids* **31**, 474–483.
- WARHOLIC, M. D., MASSAH, H. & HANRATTY, T. J. 1999 Influence of drag-reducing polymers on turbulence: effects of Reynolds number, concentration and mixing. *Expts. Fluids* **27**, 461–472.
- WEDIN, H. & KERSWELL, R. R. 2004 Exact coherent structures in pipe flow: travelling wave solutions. *J. Fluid Mech.* **508**, 333–371.
- WHITE, W. D. & McELIGOT, D. M. 1970 Transition of mixtures of polymers in a dilute aqueous solution. *ASME J. Basic Engineering* **92**, 411–418.